Heliyon 11 (2025) e41398

Contents lists available at ScienceDirect

Heliyon

journal homepage: www.cell.com/heliyon

Research article

Optimized heparin adsorption using macroporous zeolites: A comprehensive study

Katelyn R. Reid [a], Alireza Tabibi [b], Parisa Adami [c], Benson Karimi [a,*]

[a] Department of Physical and Environmental Sciences, Texas A&M University Corpus Christi, Corpus Christi, TX, 78412, USA
[b] Department of Chemistry, Isfahan University of Technology, Isfahan, 84156-83111, Iran
[c] Department of Chemistry, College of Science, University of Tehran, Tehran, Iran

ARTICLE INFO

Keywords:
Zeolite
Heparin
Porous adsorbents
Heparin adsorption
Y-zeolites adsorption
Kinetic and thermodynamics
Plasma-derived
Porcine mucosa

ABSTRACT

Heparin is a highly valuable active pharmaceutical ingredient, typically derived from porcine intestinal mucosa. Traditionally, various commercial resins have been used as adsorbents for heparin extraction; however, there has been growing interest in exploring more cost-effective adsorbents in recent years to improve heparin recovery. Zeolites, a typical aluminosilicate known for their high surface area, porosity, and thermal stability, were selected for evaluation in this study. We investigated the performance of two different zeolites, CBV901 and CBV10A, in recovering heparin. Our findings indicate that the CBV901 zeolite exhibits excellent efficiency (44 %) along with capacity (23.3 mg.g-1) for adsorption when used with porcine intestinal mucosa. A mechanistic analysis using kinetic and thermodynamic models revealed that the surface conditions were favorable for heparin adsorption. Additionally, we examined the effects of various conditions including adsorption time, as well as sorbent reusability for recovery process refinement.

1. Introduction

Plasma-derived common therapy heparin is a heterogeneous, sulfur-enriched polysaccharide biopolymer characterized by a range of molecular weights (Scheme 1) [1]. In 2023, The coronary artery disease (CAD) segment captured the largest revenue share, amounting to 23.4 %, reflecting its critical role in healthcare. CAD, the most prevalent form of heart disease, involves the narrowing of coronary arteries, reducing blood flow to the heart and leading to various clinical disorders. Renowned for its exceptional antithrombotic properties, heparin is essential for managing acute coronary events and preventing blood clots in CAD patients [2]. This medication is extensively used in the treatment of various symptoms, including acute coronary syndrome, pulmonary embolism, atrial fibrillation, and arterial thrombosis. Recent research has further identified heparin's diverse useful qualities opposing inflammation, angiogenesis, metastasis, as well as tumor growth. These multifaceted applications underscore heparin's significant value as a pharmaceutical agent [1,3–6].

The growing use of plasma in the pharmaceutical industry, evidenced by Takeda's substantial investment in plasma-derived therapies, underscores the market's expansion [2,7]. The global heparin market, valued at USD 7.56 billion in 2023, is projected to grow at a CAGR of 2.7 % from 2024 to 2030, driven by the rising prevalence of chronic diseases such as cardiovascular diseases. Key industry players, including Pfizer, LEO Pharma, GlaxoSmithKline, and Dr. Reddy's Laboratories, engage in mergers and acquisitions to

* Corresponding author.
E-mail address: Ben.Karimi@tamucc.edu (B. Karimi).

https://doi.org/10.1016/j.heliyon.2024.e41398
Received 4 October 2024; Received in revised form 2 December 2024; Accepted 19 December 2024
Available online 19 December 2024

expand their reach, further contributing to market growth [2]. The ability of distinctively recovering heparin from biological plasma fluids is a crucial skill in contemporary medical field. Recent studies are dedicated to creating novel compounds and techniques enhancing heparin adsorption's specificity as well as efficiency of the process. Advancements in heparin production, such as bio-engineered alternatives and sophisticated purification methods, underscore the industry's commitment to improving both efficacy and safety and ongoing research enhance therapeutic outcomes, reflecting the market's dynamic nature.

Generally, heparin is acquired off an intricate organic blend present in the mucosa of cattle or pig intestine [8]. Activity kicks off with the use of alkali protease enzyme subtilisin for enzymatic digestion of these animal tissues, producing a complicated blend that includes, besides heparin, proteins, nucleic acids, and various other biochemicals. The subsequent heparin recovery process involves multiple adsorption-desorption cycles, making the procedure complex and labor-intensive [9–15]. Consequently, the enzymatic digestion of natural tissue yields heparin at very low concentrations (0.01 % wt%) [16]. To address these limitations, scientists and researchers have concentrated on developing advanced adsorbents specifically engineered to selectively isolate heparin from complex mixtures. This targeted strategy aims to streamline the extraction process and optimize heparin yield. To achieve these goals, cost-effective adsorbents have been crafted using cutting-edge materials and innovative techniques. These developments have led to significant improvements in both the adsorption capacity and selectivity of the adsorbents, thereby enhancing their overall performance in the separation and purification of heparin. Currently, mass-produced adsorbent resin beads, including DEAE, Amberlite, Dowex, and Lewatit are utilized to extract heparin from animal tissues [10,12,17,18]. Despite their utility, commercial adsorbents face notable limitations, particularly in their capacity to selectively capture significant quantities of heparin, and they are often associated with high costs. To overcome these challenges, a variety of alternative adsorbents have been developed. For instance, researchers have explored the use of polymer cross-linked network structures, metal-organic frameworks (MOFs), modified silica-gel materials etc. These adsorbents are generally based on anion exchange resins that incorporate quaternary ammonium salts as their primary functional groups. The quaternary ammonium groups facilitate the adsorption of heparin through ionic interactions [13–15]. However, an effective adsorbent design requires more than functionality alone. Critical factors include controlling porosity, hydrophilicity/hydrophobicity, and the extent of cross-linking for specific applications [13]. Porosity is particularly important because it determines the resin's surface area and, thus, its adsorption capacity. Additionally, heparin adsorbents must be nontoxic and inert to avoid contaminating the isolated heparin, which serves as an active pharmaceutical agent [15,19]. Considering the exceedingly low heparin concentration of heparin in biological samples (~0.01 wt %) and the presence of competitive species such as nucleic acids, proteins, and other glycosaminoglycans (GAGs), including dermatan sulfate (DS), and chondroitin sulfate (CS), careful engineering of the adsorbent materials is crucial. This involves optimizing the adsorbent's porosity, surface chemistry, surface area, and chemical and thermodynamic stability to enhance the selectivity and efficiency of heparin extraction amidst these competing substances [20]. An effective heparin adsorbent must possess macroporous characteristics with adequately large pore sizes and substantial surface area to accommodate the sizable heparin molecules. Specifically, the pore sizes should be engineered to facilitate the diffusion and binding of heparin while maintaining high accessibility. Furthermore, the surface area should be maximized to increase the quantity of active sites available for heparin adsorption, thus enhancing the overall capacity and efficiency of the adsorbent. Optimizing these parameters is essential for improving the selective separation of heparin from complex biological mixtures [20–25].

Zeolites are porous crystalline solids formed from atoms of phosphorus, aluminum, oxygen, and silicon, exhibiting a general structure with repeated topology. Comprising an interconnected network with oxygen atoms at the corners and silicon or aluminum atoms at the center, zeolites can be natural or synthetic [26,27]. They are characterized by properties such as molecular sieve structure, ion exchangeability, and water absorbency, making them valuable in various medical applications. Notably, natural zeolites like Clinoptilolite can serve as food additives providing essential minerals and preventing environmental poisoning. Zeolites' biocompatibility has been evidenced by research showing human bone marrow stromal cells adhering and proliferating on synthesized ZSM-5 zeolite surfaces without morphological changes. Their ability to adsorb ions and toxic materials stems from their crystalline structure with porous channels, which trap charged and neutral toxins and molecules. Additionally, zeolites' unique molecular sieve allows gases and smaller molecules to pass through its crystalline network, facilitating the separation of mixed molecules based on size [26–36].

Our research specifically focuses on the utilization of zeolites engineered with larger pore sizes. Specifically, we selected CBV901, a Y-zeolite, and CB10A, a mordenite, as the adsorbents for our experiments. The rationale behind this approach is that larger pore sizes can facilitate better access to internal adsorption sites, thereby allowing for more effective capture and retention of heparin molecules. We aimed to optimize heparin adsorption by systematically varying several parameters: pH levels, the dosage of the adsorbent, process

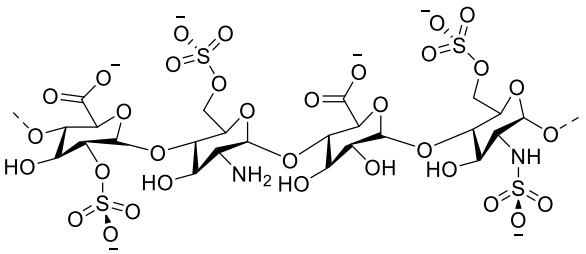

Scheme 1. Repetitive group of Heparin.

temperature and interaction time. By adjusting these variables, we sought to enhance the adsorption efficiency and selectivity of heparin, thereby improving the overall performance of the zeolite-based adsorbents in separating heparin from complex biological mixtures.

2. Results and discussion

2.1. Heparin adsorption studies

The process workflow involves adsorption of heparin on an adsorbent under biologically ideal conditions. The subsequent desorption of resulting molecule leads to procurement of heparin in pure form. Initial screenings for adhesion used solutions of pure heparin to establish baseline performance metrics, thus helping identify a zeolite adsorbent which is most efficient as per its exhibited affinity in pure heparin solutions. The selected zeolite was subsequently utilized to adsorb heparin in real biological samples. The dosage, pH parameters, temperature, and contact time were systematically moderated to develop an optimized technique of adsorption for heparin recovery from porcine mucosa, which contains a diverse array of biomolecules and enzymes. All experiments were performed in triplicate to ensure statistical robustness. Further investigations focused on evaluating the reusability of the adsorbent to assess its commercial viability. In addition, kinetic and thermodynamic analyses were performed for elucidation of underlying adsorption mechanisms, providing valuable insights into the factors influencing adsorption efficiency and selectivity. Zeolites CBV901 and CBV10A were added separately in the amount of 0.5g each into the aqueous solutions containing heparin with as concentration of 1000 mg $L^{-1}$and stirred in an incubator for 5 h at 55 °C. Following this, methylene blue method was applied to measure the rate of heparin adsorption [13,14]. In solutions of pure heparin, absorption efficiency of CBV901 is 76 % and adsorbs heparin 1.7-fold more than CBV10A (absorption efficiency 43 %). Although both CBV901 and CBV10A are macroporous adsorbents, CBV901 possesses a significantly larger surface area, approximately 1.6 times greater than that of CBV10A (700 m^2/g and 425 m^2/g respectively). This substantial difference in surface area is a critical factor contributing to the superior heparin adsorption capacity observed for CBV901. The increased surface area of CBV901 facilitates a higher number of available active sites for heparin interaction, thereby enhancing its adsorption efficiency [37,38]. Consequently, the larger surface area of CBV901 enables a more effective capture of heparin molecules from the solution compared to CBV10A, which is corroborated by the observed higher degree of heparin adsorption efficacy by CBV901. Therefore, CBV901 was analyzed further for adhesion of heparin in the live blend of mucosa obtained off pig's intestine, which is described in sections 2.1.1-2.1.6.

Heparin adsorption from an aqueous solution of pure heparin onto the surface of CBV901 was investigated further using Fourier Transform Infrared (FTIR) spectroscopy (Fig. 1). Comparative FTIR spectra were obtained for both the commercial sodium salt of heparin and the CBV901-heparin adduct. The presence of C=O asymmetric and symmetric stretching vibrations at 1618 cm^{-1} and 1421 cm^{-1} respectively in the FTIR spectrum of the CBV901-heparin adduct distinctly confirms the successful adsorption of heparin onto the CBV901 surface [39–43].

Nuclear magnetic resonance (NMR) analysis was performed to evaluate and compare the heparin isolated from CBV901 with commercially sourced heparin. As depicted in Fig. 2, the spectral peaks of the heparin eluted from CBV901 exhibit a remarkable correspondence with those of the commercially available heparin. Specifically, the methyl peaks within the N-acetyl glucosamine (GlcNAc) region for both isolated and commercial heparin appear at around 2.00 ppm [Fig. 2] [13,14,50]. This observation suggests that the CBV901 substrate has effectively adsorbed heparin from porcine mucosa.

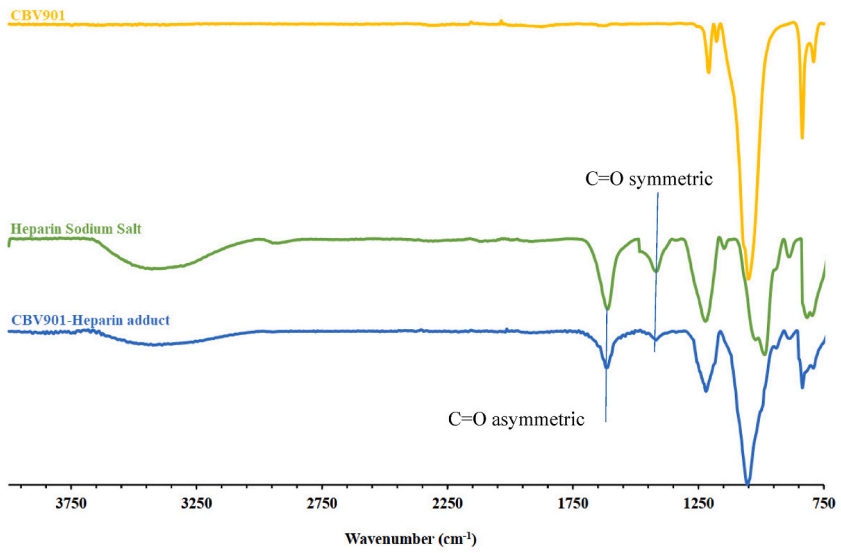

Fig. 1. The IR spectra of store-bought heparin sodium salt, CBV901, and the pre-adsorbed heparin standard on CBV901.

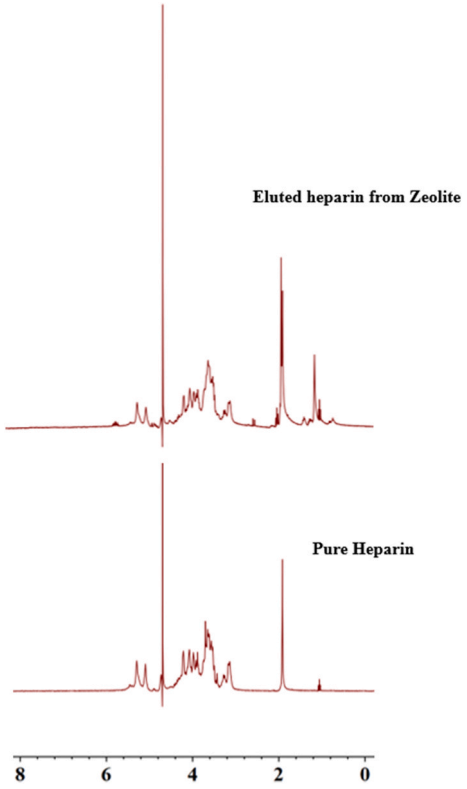

Fig. 2. ^{1}H NMR spectra (300 MHz, D_2O) of pure heparin (bottom) and real heparin (top) which is adsorbed and extracted from CBV901.

2.1.1. Adsorption dosage optimization

Investigation of adsorbent dosage's impact on consumption of heparin in real mucosa samples from pigs' intestine was conducted by varying the concentration of CBV901 between 100 and 1000 mg. The adsorption capacity reached a maximum of 23.1 mg g^{-1} with an increase in CBV901 dosage to 500 mg (Fig. 3a). At this dosage, the adsorption efficiency peaked at 44 %. However, as the adsorbent dosage was further increased beyond 500 mg, the rate of adsorption remained closely constant, while the adsorption capacity began to decline. The initial adsorption capacity surge can be attributed to the increased surface area with active sites on the CBV901 surface. Molecules such as chondroitin and dermatan sulfate in live samples of mucosa may interfere with heparin by competing for adsorption sites. This competitive binding can reduce the efficiency of adsorption at larger dosages. Additionally, an adsorption capacity decrease from 23.1 to 11.5 mg g^{-1} could be due to the increased mass (m) as per equation (11).

2.1.2. pH optimization

The medium's pH significantly affects the adsorption properties of Y-zeolite CBV901. In this study, mucosa obtained from the intestine of pigs represented the live biological sample that was utilized for conducting experiments aimed at optimizing the adsorption rate of heparin by CBV901. This optimization was achieved by modulating the pH of the sample solution within the range of 3–11. The amount of heparin adsorbed by CBV901 was quantified using an ELISA kit assay and/or a sheep plasma test.

Results demonstrated that heparin adsorption increased with pH values ranging from 3 to 8 (Fig. 3b). At low pH, other molecules present in the mucosa, compete with heparin for adsorption sites. At an optimal pH of 8, the adsorption efficiency reached its peak at 44.2 %, with an adsorption capacity of 23.3 mg g^{-1}. Beyond this pH, a slight decrease in adsorption was observed. This decline can be attributed to the deprotonation of heparin at higher pH levels, which enhances its negative charge and leads to repulsive interactions with the heparin molecules already adsorbed within the pores of the Y-zeolite. Consequently, pH 8 was identified as the optimal condition for heparin uptake by Y-zeolite CBV901.

2.1.3. Effect of temperature and duration on heparin uptake in real sample

The adhesion showcased by Y-zeolite CBV901 on heparin demonstrates a pronounced temporal increase as the heparin molecules diffuse from the solution, gradually occupying the pores of the CBV901 structure. Over a contact duration of 300 min, this process culminates in a marked enhancement in the adsorption efficiency, reaching 44.3 %, and adsorption capacity, attaining a value of 23.3 mg g^{-1}. This upward trend is substantiated by the data illustrated in Fig. 4a. Subsequently, the adsorption efficiency plateaus, indicating that the CBV901 has achieved saturation under the specific experimental conditions.

The influence of temperature on the adsorption affinity was also investigated, given its critical role in modulating this relationship.

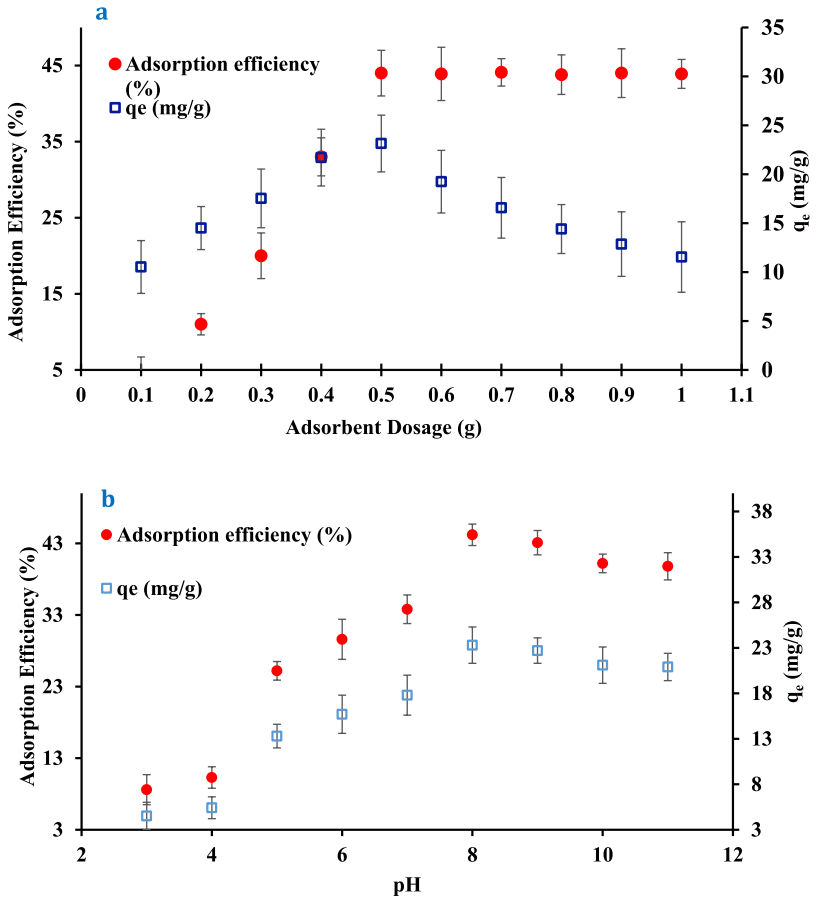

Fig. 3. The adsorption efficiency of heparin onto CBV901A was optimized by adjusting (a) adsorbent dosage (process: 25 mL of a 1315 mg L^{-1} mucosa sample at pH 8, for 300 min of contact time at 55 °C) and (b) pH (process: 0.5 g of CBV901 in 20 mL of a 1315 mg L^{-1} mucosa sample for 300 min of contact time at 55 °C).

A series of experimental repetitions in temperatures ranging between 25 °C and 75 °C were conducted. The findings, depicted in Fig. 4b, indicate that the temperature increase to 55 °C resulted in peak adsorption efficiency and capacity, achieving values of 44 % and 23.1 mg g^{-1}, respectively. This enhancement can be attributed to the reduction in solution viscosity at elevated temperatures, which facilitates more rapid diffusion of heparin molecules within the solution, thereby promoting a more efficient zeolite interactions. The cause of decline beyond 55 °C is possibly the molecular decomposition of heparin in higher temperatures.

2.1.4. Kinetic and thermodynamic studies

2.1.4.1. Kinetic study of heparin adsorption. To elucidate the heparin adsorption mechanism onto the CBV901, the influence of contact time on heparin removal was studied under optimal conditions. Typically, the reactant's concentration and the level of interactions between involved species drive the kinetics of the process. To further understand the adsorption mechanism, four kinetic models were evaluated: pseudo-first-order (Eq. (1)), pseudo-second-order (Eq. (2)), intraparticle diffusion (Eq. (3)), and Elovich (Eq. (4)).The corresponding equations for these models are as follows:

Pseudo-first-order:

$$log\,(q_e - q_t) = log\,(q_e) - \frac{k_t t}{2.303} \tag{1}$$

Pseudo-second-order:

$$\frac{t}{q_t} = \frac{1}{k_2 q_e^2} + \frac{t}{q_e} \tag{2}$$

Intraparticle diffusion:

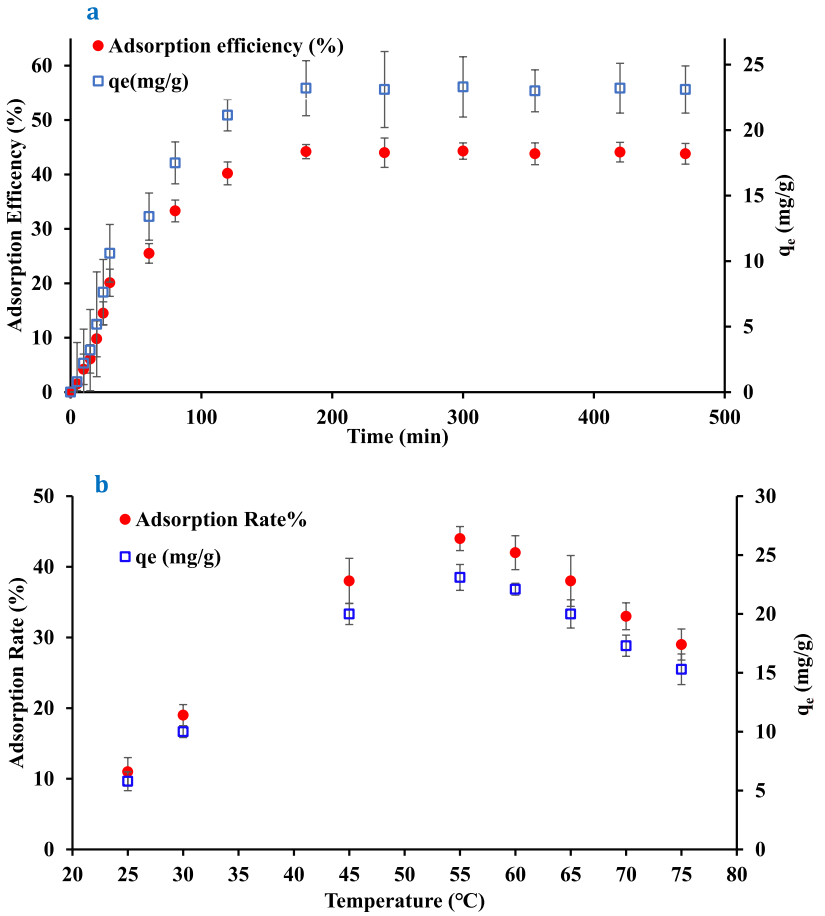

Fig. 4. The adsorption efficiency of heparin onto CBV901 was optimized by adjusting (a) contact time (parameters: 0.5 g of CBV901 in 25 mL of a 1315 mg L−1 porcine mucosa sample at pH 8 and 55 °C) and (b) temperature (parameters: 0.5 g of CBV901 in 25 mL of a 1315 mg L−1 mucosa sample at pH 8 for 300 min of contact time).

$$q_t = k_{id} t^{1/2} + I \tag{3}$$

Elovich model:

$$q_t = \frac{1}{\beta}\ln(\alpha\beta) + \frac{1}{\beta}\ln(t) \tag{4}$$

In these equations, q_t represents the adsorption capacity at time t, k_1 and k_2 are the rate constants for the pseudo-first-order and pseudo-second-order models, respectively. The term k_{id} denotes the intraparticle diffusion rate constant, α is the initial adsorption rate, and β is the desorption constant in the Elovich model. The pseudo-first order, pseudo-second order, intraparticle diffusion, and Elovich (Fig. 5 (a-d), respectively) plots shown at bellow. The results from these models, including the correlation coefficients (R^2) and other relevant constants, are detailed in Table 1. In analyzing the data, it was observed that certain data points deviated from linearity due to reaching a saturation phase. This saturation behavior is particularly evident in intraparticle diffusion and Elovich curves, where the data gradually diverges from the linear trend as it approaches a plateau. To maintain the consistency and accuracy of the linear correlation analysis, we removed the saturated data points and refitted the linear equation using only the remaining data points, which adhere to the linear trend. This approach allowed for a more reliable linear fit, ensuring that the results align more closely with the expected linear trends.

As evidenced by the highest R^2 value of 0.9794, the pseudo-first-order kinetic model provided the best fit to the experimental data. This suggests a relation of direct proportionality of the adsorption rate with the difference between the equilibrium concentration and the amount of heparin adsorbed at any given time. The pseudo-first-order model, often described by the Lagergren equation, assumes that the adsorption is a physisorption process that primarily depends on the adsorbent's available active sites. The rate constant (k_1) derived from the slope of this plot provides insights into the adsorption efficiency, indicating initial stages of rapid adsorption, followed by a gradual approach to equilibrium with the saturation of active sites. [44-49] The close resemblance between the

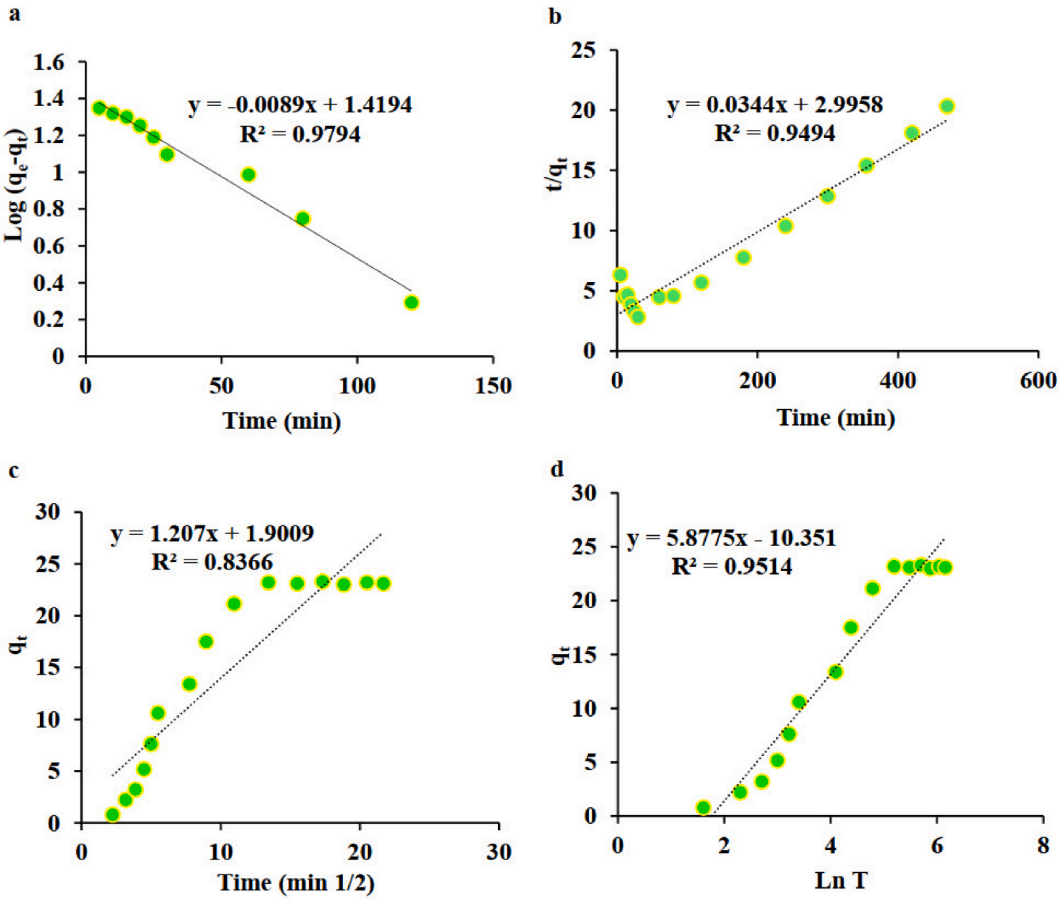

Fig. 5. The pseudo-first order (a), pseudo-second order (b), intraparticle diffusion (c), and Elovich (d) kinetic models for heparin adsorption by CBV901 in the optimal conditions.

Table 1
Kinetic model parameters calculated for adsorption of heparin on CBV901.

Model	Parameter	Value
Pseudo-first-order	K_1	0.0205
	$q_{e\ (cal)}$	26.2660
	R^2	0.9794
Pseudo-second-order	K_2	0.0005
	$q_{e\ (cal)}$	29.0690
	R^2	0.9494
Intraparticle Diffusion	K_{diff}	2.1811
	C	−3.7530
	R^2	0.9669
Elovich	β	0.1442
	α	0.9788
	R^2	0.9567

experimental and calculated q_e values further validates the applicability of the pseudo-first-order model to this adsorption system, suggesting that the adsorption process is likely driven by physisorption rather than chemisorption.

2.1.4.2. Thermodynamic study of heparin adsorption. Parameters like entropy (ΔS°), enthalpy (ΔH°), and standard Gibbs free energy (ΔG°) provide insight into the nature and feasibility of the adsorption process. To explore the thermodynamic properties of heparin adsorption onto the adsorbent, these key parameters were calculated.

Initially, the equilibrium constant (K_c) was determined using equation (5):

$$Kc = \frac{(C_0 - C_e)}{C_e} \times \frac{V}{M} \tag{5}$$

Where C_0 and C_e are the initial and equilibrium concentrations of heparin, respectively, V is the volume of the solution, and M is the mass of the adsorbent.

The Van't Hoff equation (Eq. 6) was then employed to relate the equilibrium constant to the thermodynamic parameters:

$$ln\, K_c = -\frac{\Delta H}{RT} + \frac{\Delta S^{\circ}}{R} \tag{6}$$

By plotting ln K_c against 1/T (Fig. 2. (a)), the slope and intercept were used to calculate ΔH° and ΔS°, respectively. The standard Gibbs free energy change at various temperatures was then derived from equation (7):

$$\Delta G^{\circ} = \Delta H^{\circ} - T\Delta S^{\circ} \tag{7}$$

Additionally, the activation energy (E_a) and sticking probability (S*) were estimated using 8 and 9 equations:

$$ln\,(1-\theta) = ln\, S^{*} + \frac{E_a}{RT} \tag{8}$$

$$\theta = 1 - \frac{C_e}{C_0} \tag{9}$$

The activation energy value estimated from the slope and intercept of plot of ln(1-θ) versus 1/T (Fig. 6. (b)). The thermodynamic variables were determined at various temperatures, and the resulting data are compiled in Table 2.

The thermodynamic analysis revealed several important aspects of the adsorption process. The Van't Hoff plot (Fig. 6. (a)) analysis reveals distinct thermodynamic behaviors across different temperature ranges. At lower temperatures (up to 45 °C), the Gibbs free energy (ΔG) is negative, indicating a spontaneous adsorption process. Additionally, the combination of negative enthalpy change (ΔH) and positive entropy change (ΔS) suggests that the adsorption process is exothermic and is associated with an increase in system disorder. These thermodynamic parameters collectively favor the stability and spontaneity of adsorption within this temperature range. However, as the temperature increases up to 75 °C, significant shifts in the thermodynamic parameters are observed. In this higher temperature range, ΔG becomes positive, implying that the adsorption process is no longer spontaneous. Moreover, ΔH and ΔS shift from −60.5450 to +14.2508, and +0.2172 to −0.0189, respectively, indicating an endothermic process at elevated temperatures and a decrease in system entropy. This change in thermodynamic behavior suggests that, at higher temperatures, the adsorption process requires additional energy input, and the reduction in entropy further inhibits the stability of the adsorption process, possibly due to the saturation of adsorption sites or a shift in the adsorption mechanism. This dual behavior underscores the complex nature of the adsorption process in this system and highlights the influence of temperature on adsorption spontaneity and stability.

2.1.5. Sorbet reusability

The performance of CBV901 in biological samples was remarkable, achieving an adsorption efficiency of ~44.5 % and a capacity of 23.4 mg g^{-1} under optimized pH, dosage, contact time and temperature. To assess the industrial feasibility of CBV901, we subjected the adsorbent to five cycles of adsorption-desorption. Each cycle included a stringent regeneration procedure: a thorough Milli-Q water rinsing post a 3 h saturated sodium chloride solution wash at 55 °C. The outcomes, as illustrated in Fig. 7, show that CBV901 is a highly efficient adsorbent with notable stability. Even after five rigorous adsorption-desorption cycles, CBV901 retained its performance, indicating its potential for repeated use in practical applications.

2.1.6. Sheep plasma clotting assay

For purity assessment of acquired heparin using CBV901, a sheep plasma clotting assay was conducted under optimized conditions to calculate its anticoagulant potency. A purity examination of similar nature for acquired heparin using amberlite FPA98 Cl resin was

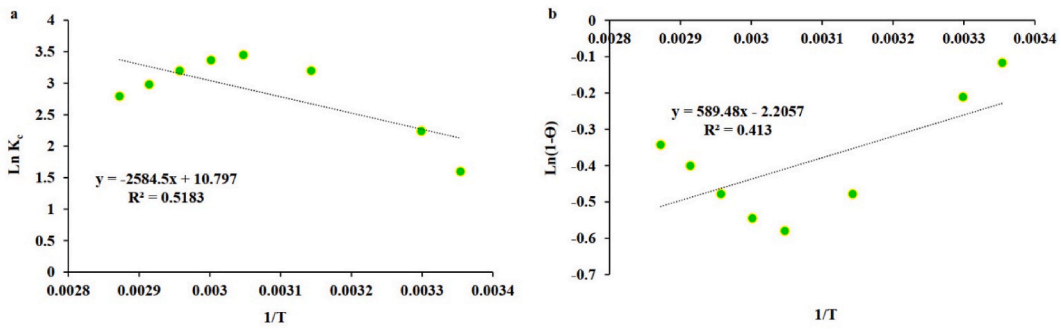

Fig. 6. The van't Hoff plot (a) and ln(1−θ) versus 1/T plot (b) of heparin adhesion on CBV901. absorbent.

Table 2
Thermodynamic parameter data for heparin adhesion on the CBV901.

ΔH° (kJ/mol)	ΔS° (kJ/mol. K)	S*	E_a (kJ/mol)	Temperature (K)							
				298.15	303.15	318.15	328.15	333.15	338.15	343.15	348.15
-60.5450	0.2172	0.0028	14.2558	ΔG(KJ/mol)							
14.2508	-0.0189	4.5727	-5.2399	-4.2102	-5.2962	-8.5540	20.4594	20.5540	20.6486	20.7432	20.8378

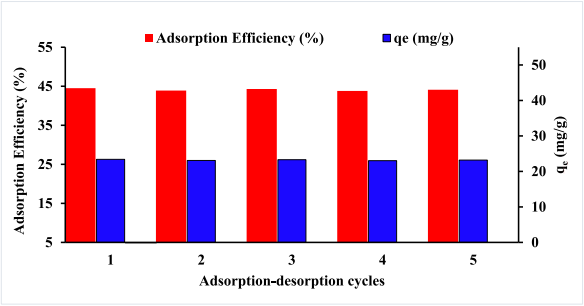

Fig. 7. Stability test of CBV901 over five adsorption-desorption heparin recovery cycle.

performed as baseline, following a previously documented procedure [50,51]. The findings from this study indicate that the anticoagulant efficacy of acquired heparin using CBV901 (61 ± 2.6) resonated closely with that of commercial amberlite FPA98 Cl resin (57 ± 3.1 U per gram of mucosa).

3. Experimental

We sourced zeolites from Zeolyst International, USA, and obtained calcium chloride, heparin sodium salt (analytical grade), hydrochloric acid (37 %), methanol, sheep plasma, sodium hydroxide and ethanol, from VWR, USA. Every chemical was utilized as is. Milli-Q water was used in sample preparation for adsorption experiments. Locally sourced intestinal mucosa contained approximately 1300 mg L^{-1} of heparin. Subtilisin enzyme was procured from STERM Company, USA. The Heparin ELISA kits and commercial Amberlite FPA98 Cl resin were sourced from MyBiosource, San Diego, CA, USA and Dow Chemical, USA respectively.

To determine the concentration of heparin in both pure and complex samples, we employed SPECTROstar nano microplate reader (BMG LABTECH). The adsorption of heparin sodium salt on the microporous zeolites were characterized using a Shimadzu IRAffinity-1 FT-IR instrument. The NMR of the sample were taken in D_2O using Bruker-Advance II 300 MHz Ultrashield NMR.

3.1. Methods

A 1000 ppm heparin stock solution was created in Milli-Q water, and the plasma of sheep and ELISA heparin kits were used to assess the efficacy and capacity of heparin adsorption by utilizing equations (6) and (7) in intestinal mucosa of pigs. This process is documented in a prior article [50].

Heparin stock solution (1000 ppm) was prepared in Milli-Q water. Sheep plasma and heparin ELISA kits were employed to evaluate the efficiency and adsorption capacity of heparin using Equations (10) and (11) in pig intestinal mucosa, as outlined in a previous study [50].

$$\textit{Adsorption efficiency}\ (\%) = \frac{(C_0 - C_e)}{C_0} \times 100 \tag{10}$$

$$\textit{Adsorption capacity}\ (q_e) = \frac{(C_0 - C_e)}{m} \times V \tag{11}$$

Here, C0 and Ce (mg L–1) represent the initial and equilibrium concentrations of heparin (determined using the ELISA kit), mass of the employed adsorbent is m (g) and the volume of mucosa solution utilized for heparin adsorption is V (L).

For evaluating zeolites adsorption abilities, the following experimental procedure was conducted: Initially, 250 mg CBV901 and CBV10A were added to 25 mL solutions of heparin sodium (concentration: 1000 ppm). These mixtures were incubated and agitated for 3 h at a constant temperature (55 °C). After the incubation period, 5 mL aliquots from individual solution were removed and filtered using a syringe filter to separate the supernatant. The supernatant's heparin concentration was measured using the spectrophotometric

method assisted by methylene blue (MB). MB, a cationic metachromatic dye, was selected for its strong affinity for heparin. For this technique, 1 mL each of heparin-containing supernatant and MB solution (10 mg L^{-1}) was combined. This combination was mixed vigorously for 10 min using a vortex mixer to ensure thorough interaction between heparin and MB. The mixture absorbance was measured subsequently using a spectrophotometric plate reader at a wavelength of 663 nm, which corresponds to unbound MB. MB forms complexes with heparin, thus reducing the concentration of free MB and consequently decreasing the absorbance intensity at 663 nm. A pre-established standard calibration curve was then used to determine heparin concentration in remaining in the solution after adsorption.

4. Conclusion

The potency of using macroporous zeolites in heparin recovery was investigated in this study. The findings demonstrate the critical role of surface area in enhancing heparin adsorption. Specifically, CBV901, with a surface area of 700 m^2/g, exhibited significantly higher heparin recovery compared to CBV10A, which has a surface area of 425 m^2/g, representing nearly a 1.6-fold increase. Additional improvement in heparin adhesion was achieved by adjusting key parameters such as absorbent dosage, pH, and temperature. As an aluminosilicate, CBV901 possesses a notably high silicon-to-aluminum ratio (SiO_2:Al_2O_3 of 80:1), which enhances its adsorption capabilities. To evaluate its performance, we compared CBV901 against previously documented silica-based adsorbents. For instance, silica-based quaternized diatomaceous earth (QDADE) demonstrated an adsorption efficiency of 31 %, while quaternized silica-gel (QMASi) achieved an efficiency of 28 % [13,14]. Among the materials analyzed, zeolite CBV901 exhibited a significant heparin adsorption efficiency of 44 %, surpassing the performance of several cationic silica-based adsorbents investigated in earlier studies. This indicates that CBV901's unique aluminosilicate structure contributes to its superior adsorption properties. The adsorption process adhered to a pseudo-first-order kinetic model, with thermodynamic analysis indicating that heparin adsorption is governed by both enthalpic and entropic contributions. The Van't Hoff analysis further revealed temperature-dependent shifts in adsorption behavior, suggesting that the process is initially driven by exothermic interactions at lower temperatures, while higher temperatures introduce entropic limitations, potentially due to site saturation or changes in the adsorption mechanism. These findings underscore the potential of CBV901 as a highly effective adsorbent for heparin recovery, paving the way for more efficient and scalable extraction methods in the pharmaceutical industry.

CRediT authorship contribution statement

Katelyn R. Reid: Writing – original draft, Visualization, Formal analysis, Data curation. **Alireza Tabibi:** Writing – review & editing, Formal analysis, Data curation. **Parisa Adami:** Writing – review & editing, Formal analysis. **Benson Karimi:** Supervision, Conceptualization.

Data and code availability

Data included in article/supplementary material is referenced in the article.

Declaration of competing interest

The authors declare that they have no known competing financial interests or personal relationships that could have appeared to influence the work reported in this paper.

Acknowledgments

B.K would like to thank Texas A & M University-Corpus Christi, Department of Physical and Environmental Sciences (PENS) for their generous support. We would also like to acknowledge the Welch Foundation for their generous support through grant number BT 0041. This funding has been instrumental in advancing our research and enabling us to achieve significant progress. Authors also would like to thank Ganesh Banerjee for reviewing and revising the manuscript.

References

[1] M.S. Lee, J. Kong, Heparin: physiology, pharmacology, and clinical application, RCM (Rapid Commun. Mass Spectrom.) 16 (3) (2015) 189–199.
[2] Heparin Market Size, Share & trends analysis report by type, by route of administration, by application, by end-use (outpatient, inpatient), by source, by region, and segment forecasts, Grand View Research, Market Analysis Report ID: GVR-3-68038-154-2 (2024 – 2030).
[3] M.d.P. Rodriguez-Torres, L.S. Acosta-Torres, L.A. Diaz-Torres, Heparin-Based Nanoparticles: An Overview of Their Applications, Journal of Nanomaterials 2018 (2018) 9780489. https://doi.org/10.1155/2018/9780489.
[4] H.H. Hwang, D.Y. Lee, Antiangiogenic actions of heparin derivatives for cancer therapy, Macromol. Res. 24 (9) (2016) 767–772.
[5] J. Atallah, H.H. Khachfe, J. Berro, H.I. Assi, The use of heparin and heparin-like molecules in cancer treatment: a review, Cancer Treatment and Research Communications 24 (2020) 100192.
[6] C. Urbinati, M. Milanesi, N. Lauro, C. Bertelli, G. David, P. D'Ursi, M. Rusnati, P. Chiodelli, HIV-1 tat and heparan sulfate proteoglycans orchestrate the setup of in cis and in trans cell-surface interactions functional to lymphocyte trans-endothelial migration, Molecules 26 (24) (2021) 7488.
[7] E. Sagonowsky, Takeda pledges close to $765M for plasma-derived therapy production site in Japan Fierce Pharma. https://www.fiercepharma.com/manufacturing/takeda-pledges-770m-plasma-derived-therapy-production-site-japan, Mar 23, 2023 5.
[8] T. Barrowcliffe, History of heparin, in: Heparin-A Century of Progress, Springer, 2012, pp. 3–22.

[9] J. Anderson, E. Saenko, Editorial I: Heparin Resistance, vol. 88, Oxford University Press, 2002, pp. 467–469.
[10] R. Flengsrud, M.L. Larsen, O.R. Ødegaard, Purification, characterization and in vivo studies of salmon heparin, Thromb. Res. 126 (6) (2010) e409–e417.
[11] M.S. Lee, J. Kong, Heparin: physiology, pharmacology, and clinical application, Rev. Cardiovasc. Med. 16 (3) (2015) 189–199.
[12] J. Vreeburg, A. Baauw, Method for preparation of heparin from mucosa, Patent No. WO2010/110654 A 1 (2010) 24.
[13] M. Karimi Abdolmaleki, A. Das, D.P. Khambhati, A. Shafiee, K. Dimas, C.A. Velazquez, S.M. Davachi, S. Choubtarash Abardeh, Efficient and economic heparin recovery from porcine intestinal mucosa using quaternary ammonium-functionalized silica gel, Bioengineering 9 (11) (2022) 606.
[14] A. Das, D.P. Khambhati, N.D. Longoria, A. Tabibi, S.M. Davachi, K. Dimas, Y. Laurencin, L. Carmona, P.Z. Avalos, M. Karimi Abdolmaleki, Modified diatomaceous earth in heparin recovery from porcine intestinal mucosa, Molecules 28 (2023) 7982.
[15] M. Karimi Abdolmaleki, D. Ganta, A. Shafiee, C.A. Velazquez, D.P. Khambhati, Efficient heparin recovery from porcine intestinal mucosa using zeolite imidazolate framework-8, Molecules 27 (5) (2022) 1670.
[16] J.-Y. Van der Meer, E. Kellenbach, L.J. Van den Bos, From farm to Pharma: an overview of industrial heparin manufacturing methods, Molecules 22 (6) (2017), https://doi.org/10.3390/molecules22061025.
[17] D.E. Hoke, D.D. Carson, M. Höök, A heparin binding synthetic peptide from human HIP/RPL29 fails to specifically differentiate between anticoagulantly active and inactive species of heparin, J. Negat. Results Biomed. 2 (1) (2003) 1–10.
[18] R.J. Linhardt, S.A. Ampofo, J. Fareed, D. Hoppensteadt, J. Folkman, J.B. Mulliken, Isolation and characterization of human heparin, Biochemistry 31 (49) (1992) 12441–12445.
[19] R.A. Haley, J.M. Ringo, H. Hopgood, K.L. Denlinger, A. Das, D.C. Waddell, J. Chem. Educ. 95 (4) (2018) 560–569.
[20] H. Eskandarloo, M. Godec, M. Arshadi, O.I. Padilla-Zakour, A. Abbaspourrad, Multi-porous quaternized chitosan/polystyrene microbeads for scalable, efficient heparin recovery, Chem. Eng. J. 348 (2018) 399–408.
[21] H. Gu, Y. Liu, L. Wang, B. Zhang, D. Yin, Q. Zhang, Monolithic macroporous hydrogels prepared from oil-in-water high internal phase emulsions for high-efficiency purification of enterovirus 71, Chem. Eng. J. 401 (2020) 126051.
[22] P.B. Welzel, M. Grimmer, C. Renneberg, L. Naujox, S. Zschoche, U. Freudenberg, C. Werner, Macroporous starPEG-heparin cryogels, Biomacromolecules 13 (8) (2012) 2349–2358, https://doi.org/10.1021/bm300605s.
[23] Y.G. Tong, B.C. Tang, Q.Q. Ma, Q. Zhao, W.C. Pan, Optimization of absorbed technology in crude heparin sodium, Appl. Chem. Ind. 44 (12) (2015) 2289–2292.
[24] S.F. Liu, Y. Liu, J. Yang, J.W. Xiao, Y.G. Li, F.P. Nie, Y. Wang, K. Tan, F.L. Tang, Study on the adsorption characteristics of FPA 98 macroporous resin to heparin sodium, Journal of Anhui Agriculture Science 41 (16) (2013) 7190–7191.
[25] M.S. Aw, S. Simovic, Y. Yu, J. Addai-Mensah, D. Losic, Porous silica microshells from diatoms as biocarrier for drug delivery applications, Powder Technol. 223 (2012) 52–58.
[26] H. Serati-Nouri, A. Jafari, L. Roshangar, M. Dadashpour, Y. Pilehvar-Soltanahmadi, N. Zarghami, Biomedical applications of zeolite-based materials: a review, Mater. Sci. Eng. C 116 (2020) 111225.
[27] L. Bacakova, M. Vandrovcova, I. Kopova, I. Jirka, Applications of zeolites in biotechnology and medicine – a review, Biomater. Sci. 6 (5) (2018) 974–989.
[28] D.G. Boer, J. Langerak, P.P. Pescarmona, Zeolites as selective adsorbents for CO2 separation, ACS Appl. Energy Mater. 6 (5) (2023) 2634–2656.
[29] Ç. Efe, L.A.M. van der Wielen, A.J.J. Straathof, High silica zeolites as an alternative to weak base adsorbents in succinic acid recovery, Ind. Eng. Chem. Res. 49 (4) (2010) 1837–1843.
[30] L. Wang, K. Ozawa, T. Komatsu, T. Ikeda, Ca2+-Exchanged ferrierite: quasi one-dimensional zeolite for highly selective and stable formation of light alkenes in catalytic cracking of n-octane, Appl. Catal. Gen. 407 (1) (2011) 127–133.
[31] S.K. Kirdeciler, E. Soy, S. Oztürk, I. Kucherenko, O. Soldatkin, S. Dzyadevych, B. Akata, A novel urea conductometric biosensor based on zeolite immobilized urease, Talanta 85 (3) (2011) 1435–1441, https://doi.org/10.1016/j.talanta.2011.06.034.
[32] N. Ninan, M. Muthiah, I.-K. Park, A. Elain, T.W. Wong, S. Thomas, Y. Grohens, Faujasites incorporated tissue engineering scaffolds for wound healing: in vitro and in vivo analysis, ACS Appl. Mater. Interfaces 5 (21) (2013) 11194–11206.
[33] Mohau Moshoeshoe, Misael Silas Nadiye-Tabbiruka, Veronica Obuseng, A review of the chemistry, structure, properties and applications of zeolites, Am. J. Mater. Sci. 7 (5) (2017) 196–221, https://doi.org/10.5923/j.materials.20170705.12.
[34] M. Matsui, Y. Kiyozumi, Y. Mizushina, K. Sakaguchi, F. Mizukami, Adsorption and desorption behavior of basic proteins on zeolites, Separ. Purif. Technol. 149 (2015) 103–109.
[35] I. Halasz, S. Kim, B. Marcus, Uncommon adsorption isotherm of methanol on a hydrophobic Y-zeolite, J. Phys. Chem. B 105 (44) (2001) 10788–10796.
[36] X. Zhang, J. Sun, J. Liu, H. Xu, B. Dong, X. Sun, T. Zhang, S. Xu, L. Xu, X. Bai, S. Zhang, S. Mintova, G. Lu, H. Song, Label-free electrochemical immunosensor based on conductive Ag contained EMT-style nano-zeolites and the application for α-fetoprotein detection, Sens. Actuators, B 255 (2018) 2919–2926.
[37] N. Jiang, R. Shang, S.G.J. Heijman, L.C. Rietveld, Adsorption of triclosan, trichlorophenol and phenol by high-silica zeolites: adsorption efficiencies and mechanisms, Separ. Purif. Technol. 235 (2020) 116152.
[38] K.-J. Kim, H.-G. Ahn, The effect of pore structure of zeolite on the adsorption of VOCs and their desorption properties by microwave heating, Microporous Mesoporous Mater. 152 (2012) 78–83.
[39] R.S. Tipson, Infrared Spectroscopy of Carbohydrates A Review, vol. 110, National Bureau of Standards Monograph, 1968.
[40] A.K. Dinda, D.R. Tripathy, A. Das, S. Dasgupta, Int. J. Biol. Macromol. 63 (2014) 107–113.
[41] D. Grant, W.F. Long, C.F. Moffat, F.B. Williamson, Infrared spectroscopy of chemically modified heparins, Biochem. J. 261 (1989) 1035–1038.
[42] A. Das, E.A. Lao, A.D. Gudmundsdottir, Photoenolization of O-methylvalerophenone ester derivative, Photochem. Photobiol. 92 (3) (2016) 388–398.
[43] D. Grant, C.F. Moffat, W.F. Long, F.B. Williamson, Carboxylate symmetric stretching infrared absorbances of chemically modified heparins, Biochem. Soc. Trans. 17 (1988) 500–501.
[44] Y.S. Ho, G. McKay, Pseudo-second order model for sorption processes, Process Biochem. 34 (1999) 451–465.
[45] J.P. Simonin, On the comparison of pseudo-first order and pseudo-second order rate laws in the modeling of adsorption kinetics, Chem. Eng. J. 300 (2016) 254–263.
[46] A. Das, S.S. Thomas, A.A. Garofoli, K.A. Chavez, J.A. Krause, C. Bohne, A.D. Gudmundsdottir, Steric demand and rate-determining step for photoenolization of di-ortho-substituted acetophenone derivatives, Photochem. Photobiol. 95 (1) (2019) 154–162.
[47] S. Azizi, M.M. Shahri, R. Mohamad, Green synthesis of Zinc oxide nanoparticles for enhanced adsorption of lead ions from aqueous solutions: equilibrium, kinetic and thermodynamic studies, Molecules 22 (2017) 831.
[48] S.K. Sarkar, D.M. Gatlin, A. Das, B. Loftin, J.A. Krause, M. Abe, A.D. Gudmundsdottir, Laser flash photolysis of nanocrystalline α-Azido-p-Methoxy-Acetophenone, Org. Biomol. Chem. 15 (35) (2017) 7380–7386.
[49] F.-C. Wu, R.-L. Tseng, R.-S. Juang, Initial behavior of intraparticle diffusion model used in the description of adsorption kinetics, Chem. Eng. J. 153 (2009) 1–8.
[50] H. Eskandarloo, M. Arshadi, M. Enayati, A. Abbaspourrad, Highly efficient recovery of heparin using a green and low-cost quaternary ammonium functionalized halloysite nanotube, ACS Sustain. Chem. Eng. 6 (2018) 15349–15360.
[51] H. Eskandarloo, M. Godec, M. Arshadi, O.I. Padilla-Zakour, A. Abbaspourrad, Multi-porous quaternized chitosan/polystyrene microbeads for scalable, efficient heparin recovery, Chem. Eng. J. 348 (2018) 399–408.